Discontinuous Galerkin Finite Element Time Domain Method for Analysis of Ferrite Circulator with Non-conforming Meshes

M. Li [1,2], X. D. Ye [3], F. Xu [1], and N. M. Luo [3]

[1] School of Electronic Science and Engineering
Nanjing University of Posts and Telecommunications, Nanjing, 210003, China

[2] Department of Electronic Information Engineering
Suqian College, Suqian, 223800, China
18800608557@163.com

[3] Department of Communication Engineering
Nanjing University of Science and Technology, Nanjing, 210094, China
yexiaodong@njust.edu.cn

Abstract ─In this paper, a Discontinuous Galerkin finite element time-domain method (DG-FETD) based on non-conforming hybrid meshes is presented for analysis of the ferrite device. The DG-FETD method with explicit difference scheme is firstly used to analyze the electromagnetic characteristics of complex medium such as ferrite material to reduce memory requirement and computational time. The recursive convolution (RC) method is applied into DG-FETD to deal with the constitutive relation of ferrite material. What's more, the non-conforming hybrid mesh method with tetrahedron-hexahedron is employed to improve the flexibility and accuracy in mesh processing and reduce the number of unknowns. Numerical results show the efficiency of the proposed method.

Index Terms ─Discontinuous Galerkin finite element time-domain method, ferrite device, non-conforming hybrid meshes.

I. INTRODUCTION

Nowadays, the analysis of the electromagnetic properties for complex medium has received much attention. The ferrite material which is regarded as complex medium is widely used for the ultra-miniature and ultra-wideband device with characteristic of non-reciprocity such as circulator and isolator. For these ferrite device, both the finite element time-domain method (FETD) [1] and the finite-difference time-domain method (FDTD) [2] can be used to analyze electromagnetic characteristics. Although the FDTD method is simple, it suffers from serious degradation when modeling curved and fine geometrical features, because staircase approximation introduces large discretization errors even when the grid size is very small. The conventional FETD method with the characteristic of flexible modeling can not form the block diagonal which must calculate a large sparse matrix inversion via solver. Fortunately, discontinuous Galerkin method has been proposed and combined with the FETD method called discontinuous Galerkin finite element time-domain (DG-FETD) method [3]-[5]. Numerical fluxes are introduced to impose the tangential continuity of the electrical and magnetic fields at the interfaces between adjacent elements. Central flux [6] and upwind flux [7] are the common ways and a comparative study of these two schemes can be found in [8]. The DG-FETD has enhanced flexibility of FETD and can support irregular non-conforming meshes constituted of various types and shapes. It also supports various basis functions in different sub-domains. Furthermore, the resulting mass matrix is a block diagonal matrix and the method can lead to a fully explicit time-marching scheme. To improve the accuracy of modeling and reduce the number of unknowns, the non-conforming meshes based on hexahedron-tetrahedron is introduced into DG-FETD [9], [10] and the information between neighboring elements is exchanged through central flux [11], [12]. To treat the ferrite material in the time-domain analysis, we usually use the recursive convolution (RC), piecewise linear RC (PLRC) and the trapezoidal RC (TRC) techniques [13]-[15]. In this letter, we introduce RC technique into DG-FETD to deal with the constitutive relation of ferrite material for the first time and further introduce the non-conforming mesh technique to RC-DGFETD which can reduce computational time, memory requirement and number of unknowns effectively. It can also improve flexibility of modeling. We will also try to implement PLRC and TRC as a future venue of research.

The theory of the non-conforming RC-DGFETD is presented in Section II. The numerical results are discussed in Section III, and the conclusion is drawn in Section IV.

II. THEORY AND IMPLEMENTATION OF THE NON-CONFORMING DG-FETD

A. Ferrite material

Permeability of the ferrite is a tensor that varies with frequency when an external magnetic field exists. We assume that an alternating magnetic field $\mathbf{H}$ and constant bias magnetic field H_0 in direction $\mathbf{y}$ is imposed on the ferrite, the total magnetization $\mathbf{M}_t$ and the total magnetic intensity $\mathbf{H}_t$ are then expressed as:

$$\mathbf{H}_t = H_0\mathbf{y} + \mathbf{H} , \tag{1}$$

$$\mathbf{M}_t = M_s\mathbf{y} + \mathbf{M} . \tag{2}$$

Where $\mathbf{M}$ denotes alternating magnetization due to $\mathbf{H}(|\mathbf{H}| \ll H_0)$. In frequency domain, when the external magnetic field is parallel to the Y axis, the permeability [16] can be expressed as:

$$\mu_r(\omega) = \begin{pmatrix} 1 + \dfrac{\omega_0\omega_m}{\omega_0^2 - \omega^2} & 0 & -\dfrac{j\omega\omega_m}{\omega_0^2 - \omega^2} \\ 0 & 1 & 0 \\ \dfrac{j\omega\omega_m}{\omega_0^2 - \omega^2} & 0 & 1 + \dfrac{\omega_0\omega_m}{\omega_0^2 - \omega^2} \end{pmatrix}. \tag{3}$$

Where $\mu_r(\omega)$ and γ denote relative magnetic permeability and gyromagnetic ratio respectively.

$\omega_0 = \gamma H_0, \omega_m = \gamma 4\pi M_s, \gamma = 1.76 \times 10^7\, rad\,/\left(s \times Oe\right)$,

$\bar{M}_s$ denotes saturation magnetization.

The Eq. (3) can be transformed into time domain expression with Inverse Fast Fourier Transforms (IFFT) method, then μ_r can be expressed as:

$$\mu_r(t) = \begin{pmatrix} \delta(t) + \omega_m\sin\omega_0 t \cdot u(t) & 0 & -\omega_m\cos\omega_0 t \cdot u(t) \\ 0 & \delta(t) & 0 \\ \omega_m\cos\omega_0 t \cdot u(t) & 0 & \delta(t) + \omega_m\sin\omega_0 t \cdot u(t) \end{pmatrix}. \tag{4}$$

B. RC-DGFETD for Ferrite material

Considering the area of the ferrite device, one can use the following Maxwell's curl equations to describe the distribution of electromagnetic fields:

$$\varepsilon_0\varepsilon_r \otimes \frac{\partial \mathbf{E}}{\partial t} = \nabla \times \mathbf{H} , \tag{5}$$

$$\mu_0(\mu_r(t)) \otimes \frac{\partial \mathbf{H}}{\partial t} = -\nabla \times \mathbf{E} . \tag{6}$$

Because the relative permittivity ε_r is independent to frequency, we focus on the derivation of (6), and (5) will be derived with formula of domain containing PML, which is introduced to truncate the boundary. We use the basis function $\mathbf{f}_i^h$ to test (6), and covert it by vector identical equation and divergence theorem.

The (6) can then be changed into:

$$\iiint_V \mathbf{f}_i^h \cdot \mu_0(\mu_r(t)) \otimes \mathbf{f}_j^h \frac{\partial h}{\partial t} dV$$
$$= -\iiint_V \nabla \times \mathbf{f}_i^h \cdot \mathbf{f}_j^e dV - \oiint_{\partial V} \mathbf{f}_i^h \cdot \mathbf{n} \times \mathbf{f}_j^e dS . \tag{7}$$

The Central-flux is employed between elements and has the following forms:

$$\mathbf{n} \times \mathbf{H}\big|_{\partial V} = \frac{1}{2}\mathbf{n} \times (\mathbf{H} + \mathbf{H}^+)\big|_{\partial V} , \tag{8}$$

$$\mathbf{n} \times \mathbf{E}\big|_{\partial V} = \frac{1}{2}\mathbf{n} \times (\mathbf{E} + \mathbf{E}^+)\big|_{\partial V} . \tag{9}$$

Where $\mathbf{E}$ and $\mathbf{H}$ represent the electrical and magnetic fields within sub-domain V, $\mathbf{E}^+$ and $\mathbf{H}^+$ represent the electrical and magnetic fields from the adjacent elements. Applying (9) into (7) leads to:

$$\iiint_V \mathbf{f}_i^h \cdot \mu_0(\mu_r(t)) \otimes \mathbf{f}_j^h \frac{\partial h}{\partial t} dV$$
$$= -\iiint_V \nabla \times \mathbf{f}_i^h \cdot \mathbf{f}_j^e dVe - \frac{1}{2}\oiint_{\partial V} \mathbf{f}_i^h \cdot \mathbf{n} \times \mathbf{f}_j^e dSe \tag{10}$$
$$- \frac{1}{2}\oiint_{\partial V} \mathbf{f}_i^h \cdot \mathbf{n} \times \mathbf{f}_j^{e+} dSe^+$$

Insertion of (4) into (10) and further use of recursive convolution leads to:

$$\frac{df_1(t)}{dt} \otimes f_2(t) = f_1(t) \otimes \frac{df_2(t)}{dt}$$

$$\mu_0\iiint_V \mathbf{f}_i^h \cdot \mathbf{f}_j^h dV \frac{\partial h}{\partial t}$$
$$+ \mu_0\iiint_V \mathbf{f}_i^h \cdot (\vec{x}\vec{x} + \vec{z}\vec{z})\mathbf{f}_j^h dV\,\mathrm{Re}[\omega_m\omega_0 e^{-j\omega_0 t}u(t) \otimes h]$$
$$+ \mu_0\iiint_V \mathbf{f}_i^h \cdot (-\vec{x}\vec{z} + \vec{z}\vec{x})\mathbf{f}_j^h dV\,\mathrm{Re}[-j\omega_m\omega_0 e^{-j\omega_0 t}u(t) \otimes h]$$
$$+ \mu_0\iiint_V \mathbf{f}_i^h \cdot (-\vec{x}\vec{z} + \vec{z}\vec{x})\mathbf{f}_j^h dV\,\omega_m h \tag{11}$$
$$= -\iiint_V \nabla \times \mathbf{f}_i^h \cdot \mathbf{f}_j^e dVe - \frac{1}{2}\oiint_{\partial V} \mathbf{f}_i^h \cdot \mathbf{n} \times \mathbf{f}_j^e dSe$$
$$- \frac{1}{2}\oiint_{\partial V} \mathbf{f}_i^h \cdot \mathbf{n} \times \mathbf{f}_j^{e+} dSe^+$$

The (11) can be converted into a matrix equation:

$$[T_h]\frac{\partial h}{\partial t} + [F1]\Omega(t) + [F2]\Gamma(t) + [Tb]h$$
$$= [P_h]e + [S_h]e + [Ss_h]e^+ . \tag{12}$$

In this paper, the perfect matched layer (PML) is constructed to truncate the computation region, DG-FETD for PML domain is also given:

$$\varepsilon(\Lambda(t)) \otimes \frac{\partial \mathbf{E}}{\partial t} = \nabla \times \mathbf{H} , \tag{13}$$

$$\mu(\Lambda(t)) \otimes \frac{\partial \mathbf{H}}{\partial t} = -\nabla \times \mathbf{E} . \tag{14}$$

Here, $\Lambda(t)$ is diagonal tensor:

$$\Lambda(t) = \vec{x}\vec{x}\left[\delta(t)+\frac{1}{2}\frac{\sigma_z}{\varepsilon_0}\mathrm{sgn}(t)\right]+\vec{y}\vec{y}\left[\delta(t)+\frac{1}{2}\frac{\sigma_z}{\varepsilon_0}\mathrm{sgn}(t)\right]$$

$$+\vec{z}\vec{z}\left[\delta(t)-\frac{\sigma_z}{\varepsilon_0}e^{-\frac{\sigma_z}{\varepsilon_0}t}u(t)\right]\theta$$

$$= (\vec{x}\vec{x}+\vec{y}\vec{y}+\vec{z}\vec{z})\delta(t)+(\vec{x}\vec{x}+\vec{y}\vec{y})\frac{1}{2}\frac{\sigma_z}{\varepsilon_0}\mathrm{sgn}(t)-\vec{z}\vec{z}\frac{\sigma_z}{\varepsilon_0}e^{-\frac{\sigma_z}{\varepsilon_0}t}u(t)$$

Using the basis function $\mathbf{f}_i^e$ and $\mathbf{f}_i^h$ to test (13) and (14) respectively and the central-flux conditions is applied between neighboring elements. Then the convolution theorem and divergence theorem is applied, (13) and (14) can be changed into:

$$\varepsilon\iiint_V \mathbf{f}_i^e\cdot\mathbf{f}_j^e dV\frac{\partial e}{\partial t}+\varepsilon\frac{\sigma_z}{\varepsilon_0}\iiint_V\mathbf{f}_i^e\cdot(\vec{x}\vec{x}+\vec{y}\vec{y}-\vec{z}\vec{z})\mathbf{f}_j^e dVe$$

$$+\varepsilon\frac{\sigma_z}{\varepsilon_0}\iiint_V\mathbf{f}_i^e\cdot\vec{z}\vec{z}\mathbf{f}_j^e dV\frac{\sigma_z}{\varepsilon_0}e^{-\frac{\sigma_z}{\varepsilon_0}t}\mu(t)\otimes e$$

$$=\iiint_V\nabla\times\mathbf{f}_i^e\cdot\mathbf{f}_j^h dVh+\frac{1}{2}\oiint_{\partial V}\mathbf{f}_i^e\cdot\vec{n}\times\mathbf{f}_j^h dSh+\frac{1}{2}\oiint_{\partial V}\mathbf{f}_i^e\cdot\vec{n}\times\mathbf{f}_j^{h+}dSh^+$$

(15)

$$\mu\iiint_V\mathbf{f}_i^h\cdot\mathbf{f}_j^h dV\frac{\partial h}{\partial t}-\mu\frac{\sigma_z}{\varepsilon_0}\iiint_V\mathbf{f}_i^h\cdot(\vec{x}\vec{x}+\vec{y}\vec{y}-\vec{z}\vec{z})\mathbf{f}_j^h dVh$$

$$+\mu\frac{\sigma_z}{\varepsilon_0}\iiint_V\mathbf{f}_i^h\cdot\vec{z}\vec{z}\mathbf{f}_j^h dV\frac{\sigma_z}{\varepsilon_0}e^{-\frac{\sigma_z}{\varepsilon_0}t}\mu(t)\otimes h$$

$$=-\iiint_V\nabla\times\mathbf{f}_i^h\cdot\mathbf{f}_j^e dVe-\frac{1}{2}\oiint_{\partial V}\mathbf{f}_i^h\cdot\mathbf{n}\times\mathbf{f}_j^e dSe-\frac{1}{2}\oiint_{\partial V}\mathbf{f}_i^h\cdot\mathbf{n}\times\mathbf{f}_j^{e+}dSe^+$$

(16)

Because parameter ω_0 and ω_m have no value in non-ferrite material region, so we can couple the matrix equations of PML region and ferrite region as follows:

$$[T_e]\frac{\partial e}{\partial t}+[T_{ep1}]e+[T_{eq1}]\varphi(t)=[P_e]h+[S_e]h+[Ss_e]h^+, \quad (17)$$

$$[T_h]\frac{\partial h}{\partial t}+[T_{hp1}]h+[T_{hq1}]\phi(t)+[F1]\Omega(t)+[F2]\Gamma(t)+[Tb]h$$
$$=[P_h]e+[S_h]e+[Ss_h]e^+$$
.(18)

Where

$$[F_1]=\mu_0\iiint_V\mathbf{f}_i^h\cdot(\vec{x}\vec{x}+\vec{z}\vec{z})\mathbf{f}_j^h dV$$

$$[F_2]=\mu_0\iiint_V\mathbf{f}_i^h\cdot(-\vec{x}\vec{x}+\vec{z}\vec{x})\mathbf{f}_j^h dV$$

$$[T_b]=\mu_0\omega_m\iiint_V\mathbf{f}_i^h\cdot(-\vec{x}\vec{x}+\vec{z}\vec{x})\mathbf{f}_j^h dV$$

$$\varphi(t)=\frac{\sigma_z}{\varepsilon_0}e^{-\frac{\sigma_z}{\varepsilon_0}t}u(t)\otimes e$$

$$\phi(t)=\frac{\sigma_z}{\varepsilon_0}e^{-\frac{\sigma_z}{\varepsilon_0}t}u(t)\otimes h$$

$$\Omega(t)=\mathrm{Re}[\omega_m\omega_0 e^{-j\omega_0 t}u(t)\otimes h]$$

$$\Gamma(t)=\mathrm{Re}[-j\omega_m\omega_0 e^{-j\omega_0 t}u(t)\otimes h]$$

$$[T_e]=\varepsilon\int_v\mathbf{f}_i^e\cdot\mathbf{f}_j^e dV, \qquad [T_{eq}]=\varepsilon\frac{\sigma_z}{\varepsilon_0}\int_v\mathbf{f}_i^e\cdot\overline{zz}\cdot\mathbf{f}_j^e dV$$

$$[T_{ep}]=\varepsilon\frac{\sigma_z}{\varepsilon_0}\int_v\mathbf{f}_i^e\cdot(\overline{xx}+\overline{yy}-\overline{zz})\mathbf{f}_j^e dV$$

$$[T_h]=-\mu\int_v\mathbf{f}_i^h\cdot\mathbf{f}_j^h dV, \quad [T_{hq}]=\mu\frac{\sigma_z}{\mu_0}\int_v\mathbf{f}_i^h\cdot\overline{zz}\cdot\mathbf{f}_j^h dV$$

$$[T_{hq}]=\mu\frac{\sigma_z}{\mu_0}\int_v\mathbf{f}_i^h\cdot\overline{zz}\cdot\mathbf{f}_j^h dV$$

(17) and (18) is discretized using leap-frog in time:

$$([T_e]+\frac{\Delta t}{2}[T_{ep1}])e^{n+1}$$

$$=\Delta t([P_e]+[S_e]+[Ss_e])h^{n-1/2}-\Delta t[T_{eq1}]\frac{\varphi^{n+1}+\varphi^n}{2}$$

$$+([T_e]-\frac{\Delta t}{2}[T_{ep1}])e^n$$
, (19)

$$([T_h]+\frac{\Delta t}{2}([T_{hq1}]+[Tb]))h^{n+1/2}$$

$$=\Delta t([P_h]+[S_h]+[Ss_h])e^{n+1}-\Delta t[T_{hp1}]\frac{\phi^{n+1}+\phi^n}{2}$$

$$-\Delta t[F1]\frac{\Omega^{n+1}+\Omega^n}{2}-\Delta t[F2]\frac{\Gamma^{n+1}+\Gamma^n}{2}$$

$$+([T_h]-\frac{\Delta t}{2}([T_{hq1}]+[Tb]))h^{n-1/2}$$
. (20)

C. Non-conforming hybrid interfaces matrix calculation

The implementation of the DG-FETD method on hybrid meshes mainly focuses on the computation of the matrix involving integrals over a hybrid interface between current elements in V and neighboring elements in V+ of the different type, it has no relationship with other matrix involving integrals over an element or an interface between two elements of the same type. So we concentrate on the calculation of such integrals of (11) as follows:

$$\frac{1}{2}\oiint_{\partial V}\mathbf{f}_i^e\cdot\mathbf{n}\times\mathbf{f}_j^{h+}dSh^+, \qquad (21)$$

$$\frac{1}{2}\oiint_{\partial V}\mathbf{f}_i^h\cdot\mathbf{n}\times\mathbf{f}_j^{e+}dSe^+. \qquad (22)$$

Where $\mathbf{f}_j^{h+}$ and $\mathbf{f}_j^{e+}$ denote basis functions of neighboring elements. There are several cases of non-conforming interfaces, two complex cases will be considered as follow. Case (a) as shown in Fig. 1 (a) corresponds to the situation where current element in V is a hexahedron and the neighboring elements in V+ are six tetrahedrons. The curved hexahedron basis function is employed in current element and edge basis functions of tetrahedral element is employed in neighboring elements [17]. One hexahedron and six tetrahedrons form the interfaces in which one quadrangular and six

triangulars intersect into six non-conforming surfaces, when we calculate the integrals of [Sse] and [Ssh] in (17) and (18) of hexahedron hybrid interface, for example, [Sse] can be calculated as:

$$\frac{1}{2}\int_s \mathbf{f}_i^e \cdot \mathbf{n} \times \mathbf{f}_j^{h+} dSh^+$$
$$= \frac{1}{2}\int_s \mathbf{f}_i^e \cdot \mathbf{n} \times \mathbf{f}_j^{h+} dS_1 h^+ + \frac{1}{2}\int_s \mathbf{f}_i^e \cdot \mathbf{n} \times \mathbf{f}_j^{h+} dS_2 h^+$$
$$+ \frac{1}{2}\int_s \mathbf{f}_i^e \cdot \mathbf{n} \times \mathbf{f}_j^{h+} dS_3 h^+ + \frac{1}{2}\int_s \mathbf{f}_i^e \cdot \mathbf{n} \times \mathbf{f}_j^{h+} dS_4 h^+ \quad , \quad (23)$$
$$+ \frac{1}{2}\int_s \mathbf{f}_i^e \cdot \mathbf{n} \times \mathbf{f}_j^{h+} dS_5 h^+ + \frac{1}{2}\int_s \mathbf{f}_i^e \cdot \mathbf{n} \times \mathbf{f}_j^{h+} dS_6 h^+$$

where $\mathbf{f}_i^e$ is curved hexahedron basis function, $\mathbf{f}_j^{h+}$ is Whitney vector basis function of the neighboring tetrahedral cells. $S_1\ S_2\ S_3\ S_4\ S_5\ S_6$ denote the hybrid interfaces of the hexahedron and the integrals in Eq. (23) are stored for each hybrid interface.

Case (b) as shown in Fig. 1 (b) corresponds to the situation where the current element in V is a tetrahedron and the neighboring elements in V^+ are hexahedrons. For this situation, $\mathbf{f}_i^e$ represents Whitney vector basis function and $\mathbf{f}_j^{h+}$ represents curved hexahedron basis function.
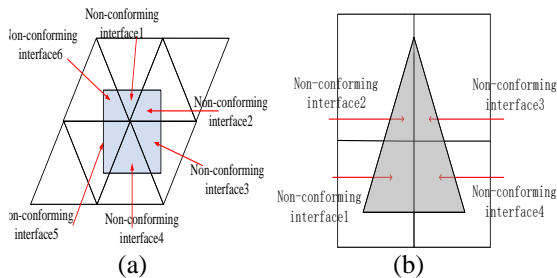

Fig. 1. (a), (b) Non-conforming hybrid interfaces formed by one hexahedron and six tetrahedrons and one tetrahedron and four hexahedrons

III. NUMERICAL RESULTS AND DISCUSSION

The numerical results are presented in this section to show the accuracy and efficiency of non-conforming RC-DGFETD for analyzing the ferrite material. Figure 2 shows the model of the Y-junction circulator, the size of the wave guide aperture is 22.86mm×10.16mm and the ferrite cylinder of the model with a radius of 3.5mm and a height of 10.16mm. Twenty layers PML are employed with a thickness of 2.5mm for each layer. The hybrid hexahedral-tetrahedral meshes and tetrahedral meshes are employed respectively as shown in Fig. 3. In the first case, the simulation domain is firstly discretized with tetrahedral grid of 1.5mm for the domain of air and hybrid hexahedral-tetrahedral grid of 0.3mm

for the ferrite part. In the second case, the model is discretized with tetrahedral grid of 1.5mm. Constant magnetic field is imposed in the direction of **y**, which is perpendicular to the propagating direction of the microwave. The magnetic intensity is 200 Oe, saturation magnetization is 1317G/4π, the relative permittivity of the ferrite material is 11.7. The excitation source used in the simulation is a Gaussian pulse with center frequency of 10GHz and bandwidth of 4GHz. The comparison of the results between different methods is shown in Figs. 4-7 and the comparison of the detailed parameters of Y-junction circulator is also listed in Table 1.
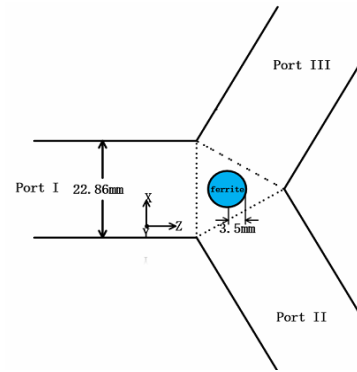

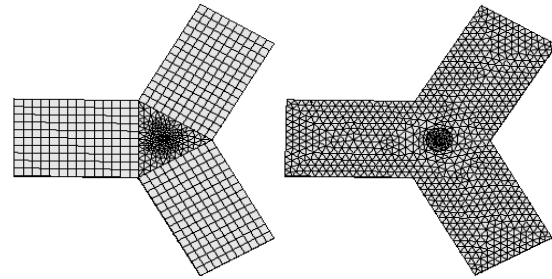Fig. 2. Geometry of the Y-junction circulator.

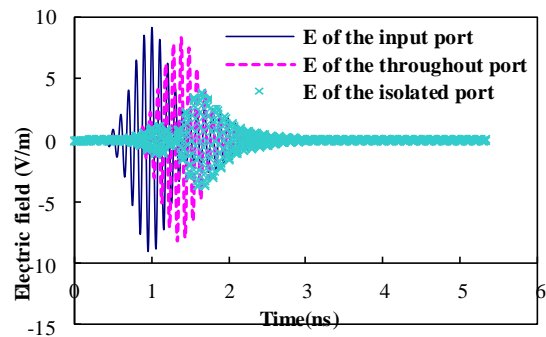Fig. 3. Hybrid and tetrahedral meshes of the Y-junction circulator.

Fig. 4. Time domain waveforms of electric field in different port of Y-junction circulator with hybrid.
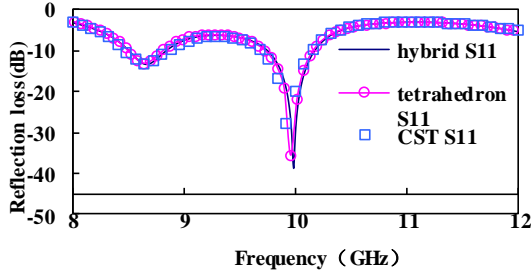
Fig. 5. Reflection loss of input port with hybrid DG-FETD and tetrahedral mesh DG-FETD and CST.
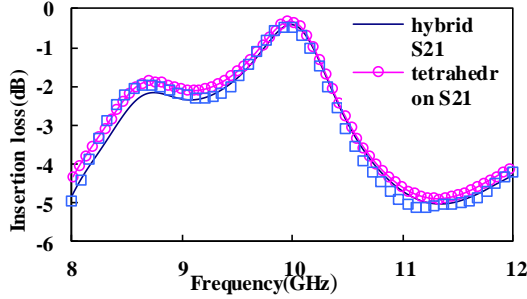

Fig. 6. Insertion loss of the throughout port with hybrid DG-FETD, and DG-FETD with tetrahedral grid and CST.
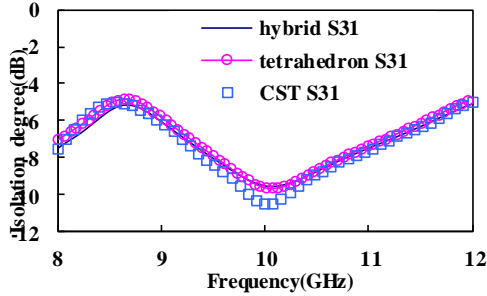

Fig. 7. Isolated degree of isolation port with hybrid DG-FETD and tetrahedral mesh DG-FETD and CST.

Table 1: Parameters of Y-junction circulator with different decomposition method

Method	Element Number	Un-knowns	Δt (ns)	Number of Time Steps	CPU Time(s)
Hybrid	21379	280259	80	18750	4049
Tetrahedral	39064	397613	50	30000	15516

From Fig. 5 to Fig. 7, a good agreement of the results between the DG-FETD and CST can be observed. The number of unknowns for the hybrid mesh is reduced compared with the tetrahedral mesh for simulations with comparable accuracy levels as shown in Table 1. What's more, the iterative time of the hybrid mesh method is much less than that of the tetrahedral mesh.

Finally, The comparison between the SETD [18] method and the DG-FETD is also given in Fig. 2 and Table 2. Both of the methods are applied to analyze the same model in the first example. A good agreement of the results between SETD and DG-FETD can be found in Fig. 8. The memory requirement and unknowns for the DG-FETD are reduced compared with the SETD as shown in Table 2. What's more, the memory requirement of the DG-FETD is also much less than that of the standard SETD.
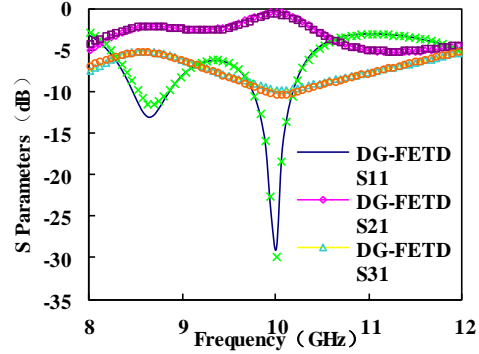

Fig. 8. The scattering parameters of Y-junction circulator with DG-FETD and SETD.

Table 2: Computational cost of the two methods

Method	Unknowns	CPU Time(s)	Memory (GB)
DG-FETD	89992	973	171MB
SETD	94971	3940	197MB

IV. CONCLUSION

This paper proposes a DG-FETD based on non-conformal meshes for the analysis of the ferrite circulator. The Discontinuous Galerkin method is presented to solve time-domain Maxwell's equation and the central-flux is used. Furthermore, the non-conformal mesh method is utilized in the DG-FETD to reduce the memory requirement and the number of unknowns. Numerical results show the efficiency of the non-conformal DG-FETD, especially for the memory requirement and iterative time.

ACKNOWLEDGMENT

REFERENCES

[1] W. H. Reed, "Triangular mesh methods for the neutron transport equation," *Los Alamos Scientific Laboratory Report LA-UR*, 1973.

[2] J. Chen and Q. H. Liu. "Discontinuous Galerkin time-domain methods for multiscale electromagnetic simulations: A review," *Proc. IEEE*, vol.

101, no. 2, pp. 242-254, Feb. 2013.

[3] S. D. Gedney, C. Luo, J. A. Roden, R. D. Crawford, B. Guernsey, J. A. Miller, T. Kramer, and E. W. Lucas, "The discontinuous Galerkin finite-element time-domain method solution of Maxwell's equations," *Appl. Comput. Electromag. Society J.*, vol. 24, no. 2, pp. 129-142, Apr. 2009.

[4] T. Lu, P. Zhang, and W. Cai, "Discontinuous Galerkin methods for dispersive and lossy Maxwell's equations and PML boundary conditions," *J. Comput. Phys.*, vol. 200, no. 2, pp. 549-580, Nov. 2004.

[5] J. Chen and Q. H. Liu, "Discontinuous Galerkin time domain methods for multiscale electromagnetic simulations: A review," *Proc. IEEE*, vol. 101, no. 2, pp. 242-254, Feb. 2013.

[6] S. D. Gedney, C. Luo, J. A. Roden, R. D. Crawford, B. Guernsey, J. A. Miller, T. Kramer, and E. W. Lucas, "The discontinuous Galerkin finite-element time-domain method solution of Maxwell's equations," *Appl. Comput. Electromag. Society J.*, vol. 24, no. 2, pp. 129-142, Apr. 2009.

[7] J. H. Lee and Q. H. Liu, "A 3-D discontinuous spectral element time-domain method for Maxwell's equations," *IEEE Trans. Antennas Propag.*, vol. 57, no. 9, pp. 2666-2674, Sep. 2009.

[8] X. Li and J. M. Jin, "A comparative study of three finite element-based explicit numerical schemes for solving Maxwell's equations," *IEEE Trans. Antennas Propag.*, vol. 60, no. 3, pp. 1450-1457, Mar. 2012.

[9] S. Dosopoulos, B. Zhao, and J. F. Lee, "Non-conformal and parallel discontinuous Galerkin time domain method for Maxwell's equations: EM analysis of IC packages," *J. Comput. Phys.*, vol. 238, pp. 48-70, Dec. 2012.

[10] S. Dosopoulos and J. F. Lee, "Interior penalty discontinuous Galerkin finite element method for the time-dependent first order Maxwell's equations," *IEEE Trans. Antennas Propag.*, vol. 58, no. 12, pp. 4085-4090, Dec. 2010.

[11] E. Montseny and X. Ferriéres, "Dissipative terms and local time-stepping improvements in a spatial high order Discontinuous Galerkin scheme for the time-domain Maxwell's equations," *J. Comput. Phys.*, vol. 227, no. 14, pp. 6795-6820, Dec. 2008.

[12] H. Xu, D. Z. Ding, and R. S. Chen. "A hybrid explicit-implicit scheme for spectral-element time-domain analysis of multiscale simulation," *J. ACES*, vol. 31, no. 4, pp. 77-82, Apr. 2016.

[13] R. J. Luebbers, "FDTD for th-order dispersive media," *IEEE Trans. Antennas Propag.*, vol. 40, no. 11, pp. 1297-1301, Nov. 1992.

[14] D. F. Kelley and R. J. Luebbers, "Piecewise linear recursive convolution for dispersive media using FDTD," *IEEE Trans. Antennas Propag.*, vol. 44, no. 6, pp. 792-797, June 1996.

[15] J. Shibayama and A. Nomura, "Simple trapezoidal recursive convolution technique for the frequency-dependent FDTD analysis of a Drude–Lorentz model," *IEEE Photonics Technology Letters*, vol. 21, no. 2, pp. 100-102, Apr. 2009.

[16] D. M. Pozar, *Microwave Engineering*. John Wiley & Sons, 2009.

[17] J. M. Jin, *The Finite Element Method in Electromagnetics*. 2nd ed., New York: Wiley, 2002.

[18] P. Shen, "Time domain spectral element analysis of complex medium microwave devices," [D] *Nanjing: Nanjing University of Science and Technology*, pp. 36-37, 2013.

Min Li was born in Shandong, China. She is currently working toward the Ph.D. degree in Nanjing University of Posts and Telecommunications. Her research interests include semiconductor simulation, RF-integrated circuits and computational electromagnetic.

Xiaodong Ye was born in Jiangsu, China. He is currently an Associate Professor with the Electronic Engineering of NJUST. His current research interests include computational electromagnetics, electromagnetic scattering and radiation.